Monte Carlo analysis of the oxygen knock-on effects induced by synchrotron X-ray radiation in the Bi2Sr2CaCu2O8+δ superconductor

Daniele Torsello, Lorenzo Mino, Valentina Bonino, Angelo Agostino, Lorenza Operti, Elisa Borfecchia, Ettore Vittone, Carlo Lamberti, Marco Truccato

Monte Carlo analysis of the oxygen knock-on effects induced by synchrotron X-ray radiation in the $Bi_2Sr_2CaCu_2O_{8+\delta}$ superconductor

PHYSICAL REVIEW MATERIALS **2**, 014801 (2018)

DOI: https://doi.org/10.1103/PhysRevMaterials.2.014801

Monte Carlo analysis of the oxygen knock-on effects induced by synchrotron X-ray radiation in the $Bi_2Sr_2CaCu_2O_{8+\delta}$ superconductor

Daniele Torsello,[1,2,3] Lorenzo Mino,[1] Valentina Bonino,[1] Angelo Agostino,[4,5] Lorenza Operti,[4] Elisa Borfecchia,[4] Ettore Vittone,[1,3] Carlo Lamberti,[4,5,6] Marco Truccato[1,5]

[1]Department of Physics, Interdepartmental Centre NIS, University of Torino, via P. Giuria 1, 10125 Torino, Italy.

[2]Department of Applied Science and Technology, Politecnico di Torino, 10129 Torino, Italy.

[3]Istituto Nazionale di Fisica Nucleare, Sez. Torino, via P. Giuria 1, 10125 Torino , Italy.

[4]Department of Chemistry, Interdepartmental Centre NIS, University of Torino, via P. Giuria 7, 10125 Torino, Italy.

[5]CrisDi Interdepartmental Center for Crystallography, University of Torino, Torino, Italy.

[6]IRC "Smart Materials", Southern Federal University, Rostov-on-Don, Russia.

Abstract

We investigate the microscopic mechanism responsible for the change of macroscopic electrical properties of the $Bi_2Sr_2CaCu_2O_{8+\delta}$ high-temperature superconductor induced by intense synchrotron hard X-ray beams. The possible effects of secondary electrons on the oxygen content via the knock-on interaction are studied by Monte Carlo simulations. The change in the oxygen content expected from the knock-on model is computed convoluting the fluence of photogenerated electrons in the material with the Seitz-Koehler cross section. This approach has been adopted to analyze several experimental irradiation sessions with increasing X-ray fluences. A close comparison between the expected variations in oxygen content and the experimental results allows determining the irradiation regime in which the knock-on mechanism can satisfactorily explain the observed changes. Finally, we estimate the threshold displacement energy of loosely-bound oxygen atoms in this material $T_d = 0.15^{+0.025}_{-0.01}$ eV.

I. INTRODUCTION

The study of the interaction between radiation and materials has been the subject of intense efforts in the past, clarifying many aspects of the fundamental mechanisms involved [1] and considering several classes of materials ranging from diamond [2] to high-temperature superconductors (HTSCs) [3]. Focusing on HTSCs, it is well-known that swift heavy ions induce well-defined columnar tracks, consisting of amorphized material [4,5], which are very effective in preventing the vortex movement and therefore in increasing the critical current [6-9]. This is due to the good matching between both shape and size of the amorphous tracks and the vortexes, which does not occur in the case of proton irradiation, because it only generates localized cascades of defects, inducing a much less effective vortex pinning [10,11].

The effect of electron irradiation has also been investigated in these materials, highlighting the formation of point-like defects[12] that cause a decrease of the critical temperature T_c and an increase of the normal state resistivity both in $YBa_2Cu_3O_{7-x}$ [13] and in $Bi_2Sr_2CaCu_2O_{8+\delta}$ (Bi-2212) [14], where energy dependent structural modifications were also observed [15].

Photons are also known to change the properties of HTSCs. For instance, γ-ray irradiation was shown to reduce T_c in Bi-based superconductors [16] and to suppress the supermodulation of Bi-2212 [17].

Concerning X-rays, it is well known that intense synchrotron beams can alter the state of the materials, but this effect is generally considered undesired radiation damage. However, interesting effects that in principle could be useful to modify materials in a controlled way, have been reported in the past [18], including for instance redox reactions [19], metal-insulator [20] and structural phase transitions [21]. Also in the case of HTSCs the irradiation with synchrotron hard X-rays has been reported to modify the normal and the superconducting properties of the target material [22,23], and this fact has recently been exploited to produce functioning electronic devices out of Bi-2212 single crystals by means of a novel nanopatterning technique [24,25]. However, the precise microscopic mechanism linking intense X-ray irradiation to the macroscopically observed properties modifications has not been clarified yet. A deeper understanding would improve the general knowledge in the field of photon-induced damage and could facilitate the optimization of this nanopatterning technique and its extension to other materials.

Since the electronic properties of superconducting oxides critically depend on the concentration of loosely-bound excess oxygen atoms, a possible origin of this effect could rely on the secondary electrons produced by the X-ray beam, which could induce atom displacement via knock-on interaction.

In recent years, an approach based on Monte Carlo simulations was proposed by Piñera *et al.* [26] to evaluate the importance of the knock-on mechanism in the damage of $YBa_2Cu_3O_{7-x}$ by γ radiation, showing that non-negligible fractions of oxygen atoms can be displaced if the threshold energy for this phenomenon is low enough.

The present paper is intended to further develop this approach and interpret some recent experimental results [22,24] concerning the irradiation of Bi-2212 microcrystals with a hard X-ray synchrotron nanobeam. The comparison between modelling and experimental results is expected to clarify whether and how oxygen knocked-on by photoelectrons can play a role in modifying the Bi-2212 properties under X-ray irradiation.

II. METHODS

A. Synchrotron nanobeam X-ray irradiation

The Bi-2212 irradiation experiments have been carried out at the European Synchrotron Radiation Facility (ESRF) in Grenoble, France. The samples discussed in the present paper refer to two different experiments. Each sample consisted of a Bi-2212 microcrystal with high aspect ratio, mounted with the *ab*-plane parallel to the surface of a sapphire substrate and provided with electrical contacts which allowed performing four-probe electrical measurements [27,28]. The first experiment was performed at the EH2 experimental hutch of the former ID22 beamline, where two samples have been irradiated. Sample WBAP13 underwent three irradiation sessions, whereas sample WBAP14 was irradiated in two sessions. In order to monitor the effect of irradiation on the electrical properties, crystals were characterized off-line between each irradiation session. Details of the sample preparation process and of irradiation results have already been published elsewhere [22,24]. The second experiment was performed at the new ID16B beamline on samples WBVB05 and WBVB10. In this case the setup allowed on-line monitoring of the sample resistance during irradiation, so that the effect of each irradiation session could be clearly identified by comparing the resistance values before and after irradiation without any sample removal. In both cases a pink beam has been used, centered at hv = 17.05 and 17.50 keV, respectively, and its full width half maximum (FWHM) sizes in each direction were determined by means of the knife-edge method.

TABLE 1. Beam energy hv, beam size, photon flux F, single point irradiation time Δt and irradiation mesh spacing for the different samples. The mesh spacing refers to the distances between adjacent irradiation points in the irradiation mesh averaged over the sessions (see Δy and Δz in Fig. 1). All of the irradiations have been carried out in air at room temperature ($T \approx 295$ K).

Sample	**Energy hv (keV)**	**Beam size (nm^2)**	**Photon flux F (s^{-1})**	**Irradiation time Δt (s)**	**Mesh spacing $\Delta y \times \Delta z$ (nm^2)**
WBAP13	17.05	117 × 116	1.9×10^{11}	4-10	157 × 378
WBAP14	17.05	117 × 116	1.9×10^{11}	10	122 × 425
WBVB05	17.50	50 × 70	$0.2 – 2.7 \times 10^{11}$	0.2-10	50 × 70
WBVB10	17.50	50 × 70	$1 – 2.8 \times 10^{10}$	0.2-12	50 × 70

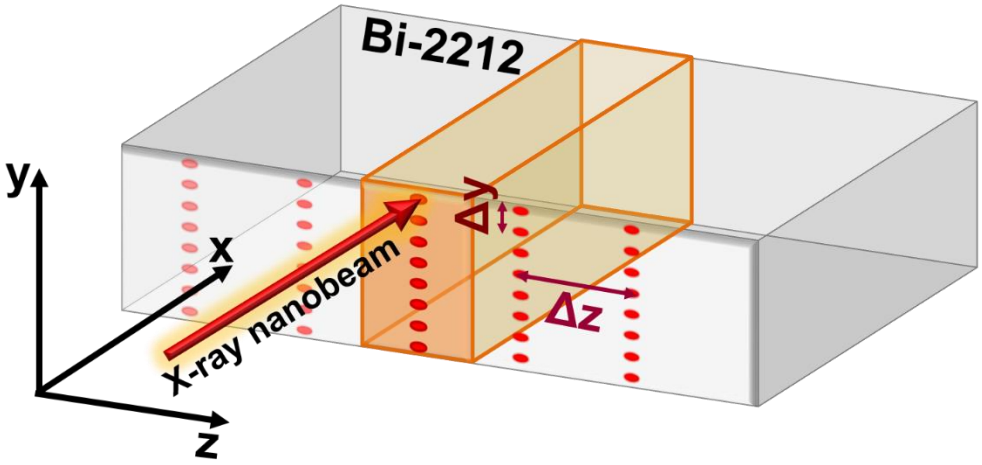

FIG. 1. Typical geometry (not on scale) of the irradiation mesh for each irradiation session. The beam is pointed onto the Bi-2212 sample on a spot for the selected irradiation time Δt, then moved in the y direction to a second spot and so on. After a row is traced across the whole crystal, the beam is moved along the z direction and the next row is drawn. Δy and Δz represent the mesh spacing between irradiation points in the two directions, respectively. The orange box represents the elementary unit on which calculations are carried out for each experimental setup, as explained in the text. The crystal *a*-, *b*-, and *c*-axes are parallel to the z, x, and y direction, respectively.

The main features of the irradiation processes used in the two experiments are reported in Table 1 and the corresponding geometry is illustrated in Fig.1.

For the comparison with the simulation results, the relevant quantity extracted from both experiments is the room temperature resistivity of the irradiated part of the sample after each irradiation step. See Supplemental Material at [URL will be inserted by publisher] for the experimental electrical data used to extract the resistivity values (Figures S1 and S2).

B. Monte Carlo simulations of the irradiation process

For each sample and irradiation session, a Monte Carlo simulation was carried out using the MCNP6 code [29] [30], which gives directly the spatial and energy distribution of the fluence of photogenerated electrons in the sample. It is worth noticing that MCNP6 code does not take into account the crystal structure of the solid, which is considered amorphous. However, this does not affect our result accuracy because of the energy cutoff of 1 keV used by MCNP6 for electron transport, which is a value much higher than the energy scale where band structure effects could play a role. Consequently, the input needed for the simulation is just the sample elemental composition and geometry (see Supplemental Material at [URL will be inserted by publisher] for sample description, Table S1), and the characteristics of the beam (see Table 1). The resolution in energy of the fluence distribution was set to 1 keV and the sample was subdivided into elementary volumes called voxels whose size was 50x50x50 nm^3. The fluence per energy unit occurring in the i-th voxel centered in (x_i,y_i,z_i) for any position p of the beam $\Phi^p_e(x_i,y_i,z_i,E)$ has been evaluated by MCNP6 as the average track length of the photogenerated electrons in the voxel, divided by its volume. For each sample and session, the spatial and energy distribution of the fluence of the whole irradiation process $\Phi_e(x_i, y_i, z_i, E)$ was reconstructed by simulating separately the incidence of the X-ray beam at all of

the different points *p* of the experimental irradiation mesh (Fig. 1) and adding up the resulting $\Phi^p_e(x_i,y_i,z_i,E)$ values in each voxel: $\Phi_e(x_i, y_i, z_i, E) = \sum_p \Phi_e^p(x_i, y_i, z_i, E)$. This procedure follows from the assumption that irradiations at different points are independent one from the other. All the results are presented for the physically relevant elementary unit of the sample (represented as the orange box in Fig. 1), which was chosen considering the translational symmetry of the experiment along the z axis but not along the y direction, because in this case the edge effects are not negligible due to the much smaller size of the crystal along y. It should be noted for clarity that this unit cell is composed of many voxels in each direction, and therefore the spatial distribution of the electrons can be studied. The lines corresponding to the intersections between the sample and the beam axes of an irradiation row lie in the xy mirror plane of this elementary unit, resulting in the fluence of the electrons being maximum there and decreasing for the other xy planes towards the borders. The interaction effects between neighboring elementary units have been considered by simulating also the neighboring irradiation rows that are closer than the lateral spread of the photogenerated electrons, because in this case they could significantly contribute to the fluence. The elementary unit is generally different for each irradiation session since it depends on the geometry of the irradiation mesh.

III. RESULTS AND DISCUSSION

A. Monte Carlo simulation results

The first step of our model to evaluate the importance of the oxygen knock-on process during synchrotron X-ray irradiation consists in computing the amount of photoelectrons generated by the nanobeam. Fig. 2 shows the typical energy distribution of the total electron fluence $\Phi_e(E) = \sum_i \Phi_e(x_i, y_i, z_i, E)$ in the elementary unit of the sample, calculated as the spatial sum over all of the voxels (x_i,y_i,z_i) in this region.

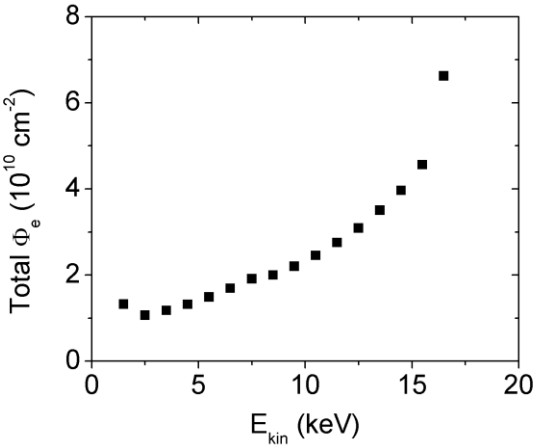

FIG. 2. Typical energy distribution of the total electron fluence $\Phi_e(E)$ calculated over an elementary unit of the sample (see Fig. 1). The results are normalized per source particle of the simulation and are therefore relative to a single incident photon. The parameters employed for this simulation correspond to the experimental conditions of the third irradiation session on sample WBAP13 ($h\nu$ = 17.05 keV) and the results are qualitatively identical to all of the other studied sessions.

It can be noticed that the energy distribution $\Phi_e(E)$ is maximum for electron energies close to the one of the X-ray beam, as expected. The spatial distribution of these electrons corresponding to the maximum ($16 < E \leq 17.05$ keV) is reported in Fig. 3a; for comparison Fig. 3b also shows the spatial distribution for electrons with energy between 7 and 8 keV, whose behavior is representative of all

the other energy ranges. From the shape of the contour lines, it is visible that higher energy electrons keep the directionality of the beam, whereas for lower energy electrons the diffusive behavior prevails. It is also visible the decrease of the fluence of electrons when moving along z from the center of the elementary unit (map 1), where the irradiation points are centered, to its border that corresponds to the point of maximum distance from any irradiation row (map 5). The same decrease is also observed for the symmetrically equivalent sections along the z direction (not presented in the figure), as expected. The electron fluence distribution of each irradiation session can be used to calculate the expected fraction of atoms removed via the knock-on mechanism, as explained in the next section.

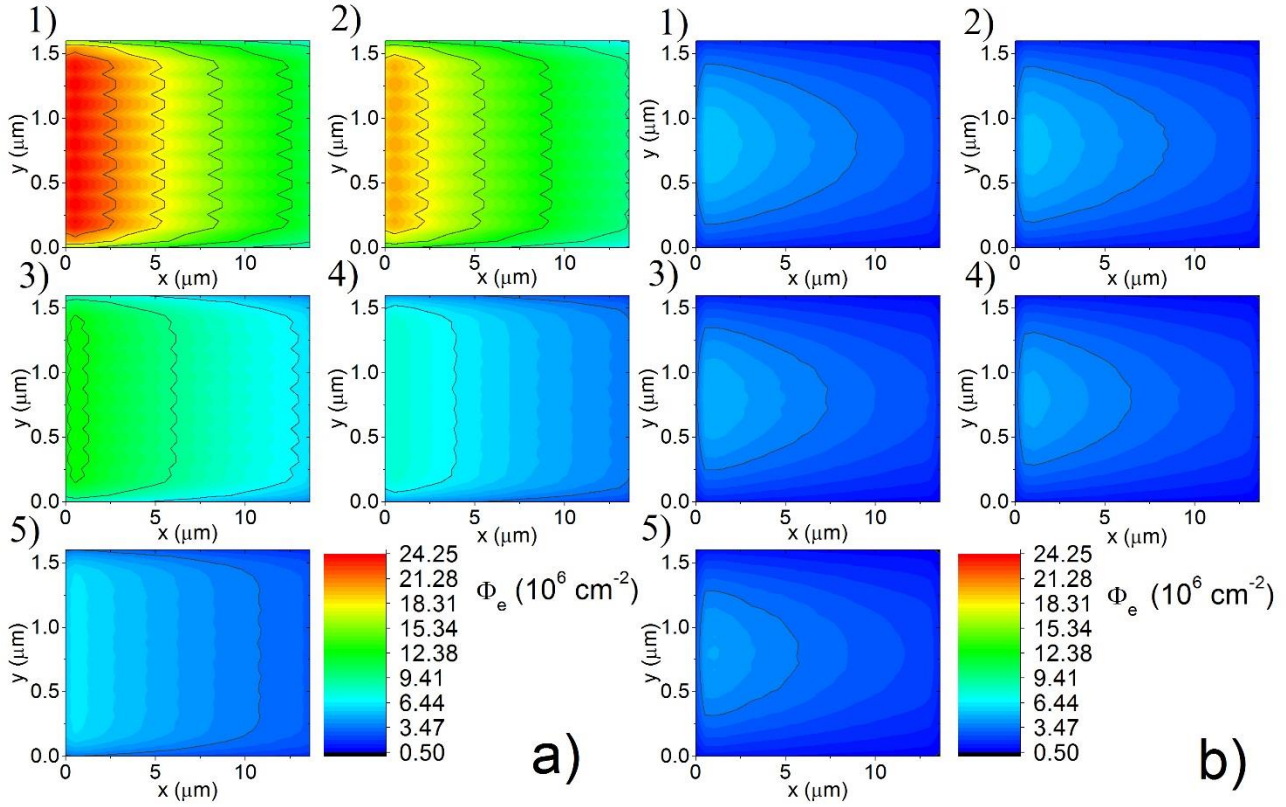

FIG. 3. Spatial distribution of the total electron fluence $\Phi_e(x_i,y_i,z_i,E)$ for electrons with kinetic energy E between 16 and 17.05 keV (a), and between 7 and 8 keV (b), in the case of the data of Fig. 2. X-rays come from left to right and impinge the crystal at x=0. Each electron distribution map is a xy-plane cross-section with a thickness of 50 nm in the z direction, centered at an irradiation row position $z=z_0$ (1), at $z=z_0$ +50 nm (2), at $z=z_0$ +100 nm (3), at $z=z_0$ +150 nm (4), and at $z=z_0$ +200 nm (5). The results are normalized per source particle of the simulation and are therefore relative to a single incident photon.

B. Calculation of displaced oxygen fraction

Knock-on damage refers to atom displacement caused by momentum and kinetic energy transfer from an electron to an atom that is initially at rest, and can be described by the integral cross section derived by Seitz and Koehler [31], which is fairly accurate for light atoms (Z<40):

$$\sigma_{PKA} = \frac{\pi Z_a^2 r_0^2}{\beta^4 \gamma^2}\left\{\left(\frac{T_m}{T_d}-1\right) - \beta^2 ln\left(\frac{T_m}{T_d}\right) + \pi\alpha\beta\left[2\left(\sqrt{\left(\frac{T_m}{T_d}\right)}-1\right) - ln\left(\frac{T_m}{T_d}\right)\right]\right\} \quad (1)$$

where Z_a is the atomic number of the target atom, r_0 is the electron classical radius, $\alpha = Z_a/137$, β is the ratio of electron velocity to light velocity and γ is the Lorentz factor. The cross section is strongly dependent on two parameters: the threshold displacement energy T_d and the maximum kinetic energy of the recoil atoms T_m, which depends on the electron energy E as $T_m \approx 2E(E+2mc^2)/Mc^2$ (where mc^2 is the electron rest energy and M the atomic mass of the atom). The maximum value for T_m in our simulations is T_m =2.44 eV, corresponding to E = 17.5 keV.

As shown by Piñera *et al.*[26], loosely-bound light atomic species like oxygen can be displaced by high energy photons in HTSC. In Bi-2212 the most loosely bound atoms are represented by the interstitial oxygen (iO) atoms lying in the Bi-O layers of the crystal structure, which are responsible both for its incommensurate modulation [32] and for changes in the critical temperature and normal state resistivity [33] [34]. Therefore, adapting Piñera's approach to the case of Bi-2212, the local number density of displaced interstitial oxygen atoms $n_{DPA}(x,y,z)$ can be evaluated from the spatial and energy fluence distribution of photogenerated electrons $\Phi_e(x,y,z,E)$ by convoluting it with the Seitz-Koehler cross section σ_{PKA}:

$$n_{DPA}(x,y,z) = n_{io} F \Delta t \int_{E_c}^{h\nu} \sigma_{PKA}(E) \Phi_e(x,y,z,E) dE \quad , \qquad (2)$$

where n_{io} is the number density per unit volume of interstitial oxygen atoms before irradiation, $E_c = \sqrt{(mc^2)^2 + \frac{Mc^2 T_d}{2}} - mc^2$ is the minimum kinetic energy of the electrons needed to displace the target, and $F\Delta t$ is the total number of photons impinging each irradiation point. It is worth noticing that in Eq.(2) the damage function of the Kinchin–Pease model [35] has been implicitly assumed equal to 1 for two reasons: i) it is possible to show that the average kinetic energy of the recoiling oxygen atoms T_{av} is always $T_{av} > T_d$ when $E > E_c$ for the typical T_d values involved in the problem (see below), and ii) it is very unlikely that primary knock-on iO atom can generate a secondary displacement of another iO atom because of the fact that they are very diluted in the Bi-2212 material (one iO atom every 4-5 crystal unit cells, on the average). On the other hand, secondary atomic displacements due to iO atoms impinging of other atomic species are very unlikely because of the much higher T_d values expected in this case[26].

Before carrying out this calculation, a value for the threshold displacement energy T_d has to be selected. This is a crucial point since the cross section σ_{PKA} reported in Eq.(1) is strongly dependent on T_d . See Supplemental Material at [URL will be inserted by publisher] for this dependence (Fig. S3). Unfortunately, this quantity is extremely difficult to be determined both experimentally and from simulations, since its definition is somehow ambiguous. Recalling that T_d is the minimum energy needed to induce a permanent displacement of the target atom from its lattice position, it is important to note that, depending on the time-scale, a certain displacement could be considered permanent or not. Therefore T_d is not an intrinsic material property [36]. Moreover, no well-established value of T_d has been determined so far for the iO atoms of Bi-2212. Due to data shortage, just a few results can be considered for reference purposes. For instance, on one hand, the *ab*-plane diffusion of iO atoms has been studied by Runde *et al.* [37] over distances of the order of 1-10 μm and time scales of 1-6 hours, determining an activation energy for the process equal to 0.93 eV. According to the authors, this amount of energy simply represents the energy required for the motion of the iO atoms over these space and time scales, including no formation energy of the interstitials. On the other hand, Bandyopadhyay *et al.* [38] [39,40] studied the oxygen out-diffusion induced in polycrystalline Bi-2212 by 40 MeV α-irradiation and showed that by assuming in the TRIM program a binding energy for the iO atoms equal to 0.073 eV it was possible to explain their experimental data by means of the

oxygen knock-on process. In order to keep a general validity of our study, we have employed both values to obtain the number density of the displaced atoms.

The calculated $n_{DPA}(x,y,z)$ divided by the number density of interstitial oxygen atoms yields the spatial distribution of the *fraction* of displaced interstitial oxygen atoms $f_{ad}(x,y,z)$, which is presented in Fig.4. The sensitivity of the model to T_d is visible in the magnitude of the displaced fraction that increases by more than a factor of 50 when using the lower T_d value. Jagged contour lines are clearly visible in the *xy* cross-sections closer to the irradiation row, and this non-homogeneity of the displacement is due to the quite large spacing along the y direction between the points of the irradiation mesh. It is also still visible a decrease of f_{ad} along the z direction from the center of the elementary unit to its border, which is simply reflecting the behavior already observed for the spatial distribution of the total electron fluence $\Phi_e(x_i,y_i,z_i,E)$.

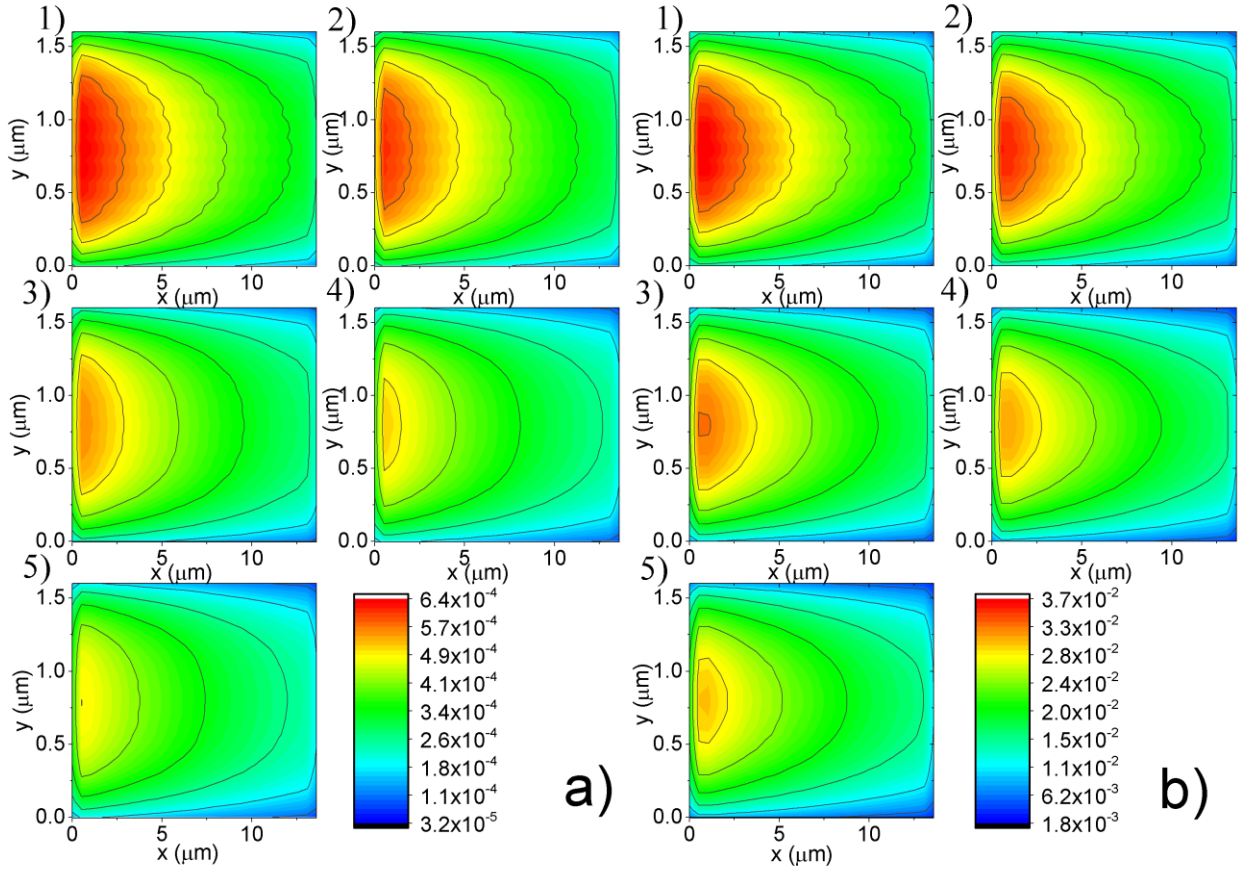

FIG. 4. Spatial distribution of the fraction of displaced interstitial oxygen atoms $f_{ad}(x,y,z)$ corresponding to the data of Fig. 2 and 3, obtained using (a) T_d = 0.93 eV and (b) T_d = 0.073 eV. X-rays come from left to right and impinge the crystal at x=0. The maps are xy-plane cross-sections with a thickness of 50 nm in the z direction, centered at an irradiation row position z=z_0 (1), at z=z_0 +50 nm (2), at z=z_0 +100 nm (3), at z=z_0 +150 nm (4), and at z=z_0 +200 nm (5). Color scale is linear. Black solid contour lines are spaced by about (a) 8×10^{-5} and (b) 4.6×10^{-3}.

C. Comparison with experiments

To evaluate if the knock-on interaction mechanism can explain the experimentally observed effects, a comparison between the simulated and experimental data is necessary. Unfortunately, the interstitial oxygen content δ of Bi-2212 is not easily accessible from a direct measurement, but can be estimated

from the room temperature *ab*-plane resistivity values $\rho_{ab}(RT)$ recorded before and after each irradiation session.

Indeed, Watanabe *et al.* [33] investigated a series of Bi-2212 single crystals and reported for the same samples both the δ content and the room temperature *ab*-plane resistivity $\rho_{ab}(RT)$, which covers a range from 2.5 to about 9 Ω μm. Another very interesting and extensive data set is presented in a paper by Kendziora *et al.* [41], where highly underdoped samples with $\rho_{ab}(RT)$ values between about 2.5 Ω μm and 1×10^5 Ω μm are presented. Although the latter results clearly show that $\rho_{ab}(RT)$ values increase in an exponential way with the decrease of the Bi-2212 doping level, they have been obtained not via a direct oxygen removal, but via cation substitution of Y for Ca, making this information not completely homogeneous with both Watanabe's results and our experiments. Therefore, we have discarded the data set by Kendziora *et al.* [41] for a direct comparison with our experiments, retaining only the qualitative information of an exponential relationship between $\rho_{ab}(RT)$ and the interstitial oxygen content δ. Consequently, the data from Watanabe *et al.* [33] have been used to obtain a reference curve for δ as a function of $\rho_{ab}(RT)$ by means of an exponential fit. See Supplemental Material at [URL will be inserted by publisher] for the determination of the reference curve (Fig. S4). Since the resistivity range covered by this reference data set spans approximately from 2.5 to 9 Ω μm, it can be safely assumed that the δ contents estimated from this reference curve are reliable for resistivity values $\rho_{ab}(RT)$ close to this range. Unfortunately, $\rho_{ab}(RT)$ reached values equal to several hundreds of Ω μm in samples WBVB05 and WBVB10, so that their δ values are necessarily extrapolated. However, these $\rho_{ab}(RT)$ values still lie in the range investigated by Kendziora *et al.* [41].

The δ values obtained via the reference curve from the experimentally determined values of $\rho_{ab}(RT)$ (for each sample and irradiation session) have been used for a comparison with the corresponding δ values obtained from the knock-on interaction model for both T_d values.

It is worth stressing that each Monte Carlo simulation yields a spatial distribution $f_{ad}(x,y,z)$ of the fraction of interstitial oxygen displaced by the knock-on interaction in the irradiated area, whereas on the other hand only a single value of f_{ad} is needed to make a comparison with the observed electrical properties variations, whose measurements represent an average over macroscopic portions of the samples. Therefore, the spatial average $f_{m,ad}$ of the $f_{ad}(x,y,z)$ values in the elementary unit of each irradiation session has been calculated for this comparison. Assuming that no other mechanism contributes to the oxygen displacement, the final interstitial oxygen δ_f content after each irradiation session can be evaluated from the initial one δ_i as $\delta_f = \delta_i(1-f_{m,ad})$. This equation assumes that displaced oxygen atoms can leave the material, or at least can move to some positions where they are electronically inactive. The fact that displaced iO atoms are able to exit Bi-2212 was experimentally confirmed by Bandyopadhyay *et al.* measuring the oxygen content of polycrystalline Bi-2212 samples by means of iodometry after α-irradiation [38-40].

Fig. 5 shows the comparison between experimentally determined and numerically modelled oxygen contents δ for all the irradiation sessions on samples WBAP13, WBAP14 (a), WBVB05 and WBVB10 (b). Since the interest is in the variations of the oxygen content caused by the X-ray irradiation and not in the exact δ values, uncertainties have been calculated considering all of the quantities that rigidly shift the $\delta(\Phi_{ph})$ curve as exact numbers.

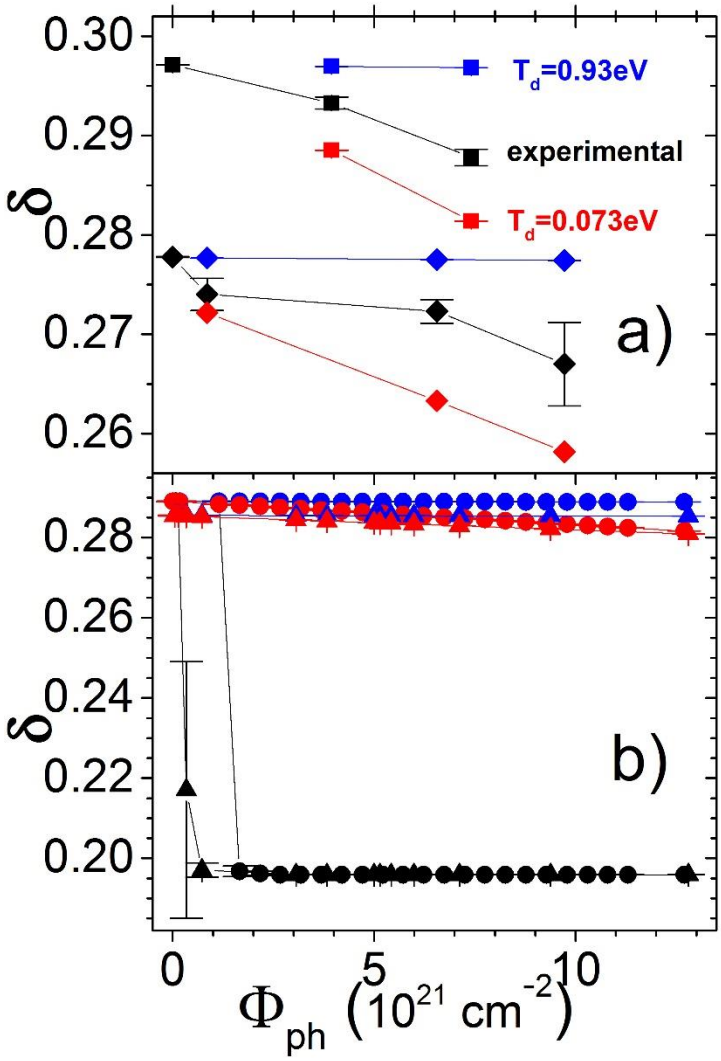

FIG. 5. Comparison between experimental and simulated δ values as a function of the photon cumulative fluence Φ_{ph} for all the irradiation sessions on samples (a) WBAP13 (diamonds) and WBAP14 (squares), and (b) WBVB05 (circles) and WBVB10 (triangles). Black symbols indicate the experimental values, blue represents the values from simulations with T_d = 0.93 eV and red the values from simulations with T_d = 0.073 eV.

The experimentally observed gradual decrease of δ in samples WBAP13 and WBAP14 (Fig. 5a) denotes a clearly different behavior from the one of samples WBVB05 and WBVB10 (Fig. 5b), in which a sudden decrease is followed by a saturation at the asymptotic value of the fit. In the former regime, the numerical simulation results for T_d = 0.073 eV and T_d = 0.93 eV overestimate and underestimate, respectively, the change in δ suggesting that a satisfactory agreement could be achieved with an intermediate T_d value. Conversely, in the latter case both T_d values give a large underestimation of the observed changes. The T_d value for which the best agreement is achieved has been estimated to be $T_d = 0.15^{+0.025}_{-0.01}$ eV by minimizing the χ^2 of the simulations with respect to the experimental values for samples WBAP13 and WBAP14 (inset of Fig. 6). This result is about the double of the T_d = 0.073 eV value that was required to explain the oxygen out-diffusion in α-irradiation experiments[38-40], and also compares favorably to recent DFT calculations showing that a 0.2 eV energy difference exists between the stability points and other relative minima positions for iO atoms in the Bi-O layer [42]. The δ values calculated with the best estimate T_d = 0.15 eV are in

excellent agreement with the experimental results (see Fig. 6). The fact that the model is able to explain the changes observed in the experiment on samples WBAP13 and WBAP14, but not in the one corresponding to samples WBVB05 and WBVB10 could be related to the spacing of the irradiation mesh that is very different in the two cases. In the former the mesh spacing is about three times larger than the beam size, whereas in the latter they are identical (see Table 1). In this respect, it is worth stressing that our simulation procedure firstly calculates the oxygen displacement distribution independently induced by each irradiation point as if the X-rays were impinging on pristine Bi-2212, and then the final oxygen displacement distribution is obtained for every irradiation session by adding the partial results from all of the corresponding irradiation points. However, during an experimental session it is possible that a neighboring irradiation point has already produced some damage at the site where we want to perform a simulation, especially if the irradiation points are closely spaced. This could represent a severe problem for our simulation procedure if the already existing damage is significant and the damage effects do not simply add in a linear way. Therefore, our impossibility to reproduce the experimental results of samples WBVB05 and WBVB10 suggests that this is the case, implying that our simulation method cannot be applied neither to closely spaced nor to heavily irradiated samples.

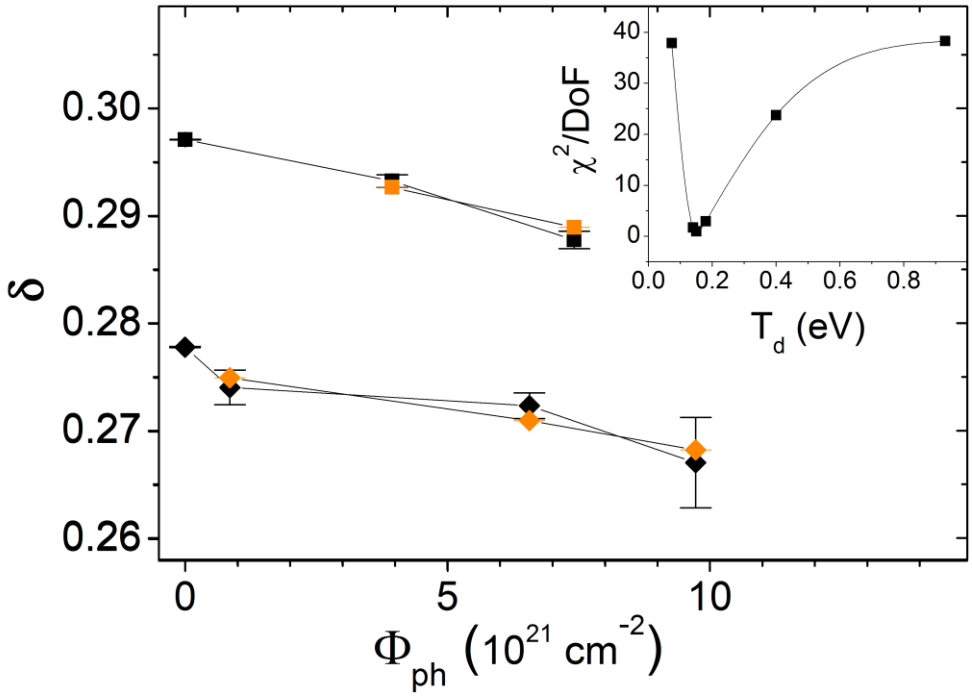

FIG. 6. Comparison between experimental data (black) of samples WBAP13 (diamonds) and WBAP14 (squares) and simulated values (orange) obtained for the value of T_d corresponding to minimization of χ^2 ($T_d = 0.15^{+0.025}_{-0.01}$ eV). The inset shows the normalized χ^2 as a function of T_d quantifying the agreement between experimental and simulated values calculated over the whole set of irradiations for samples WBAP13 and WBAP14. The solid curve is a guide for the eye.

IV. CONCLUSIONS

We have presented a Monte Carlo procedure for the analysis of the effects of X-ray irradiation on Bi-2212 in the framework of the knock-on model of interstitial oxygen atoms by secondary electrons. The MCNP6 numerical simulations allow estimating the spatial and energy distribution of the

secondary electrons generated in the material by the X-ray beam. After a complete reconstruction of each irradiation session, it has been possible to compute the expected variation of the interstitial oxygen content. This quantity has been compared to the experimental variation of the oxygen content estimated from the change in room temperature resistivity.

We have identified two different regimes, distinguished by the density of points of the irradiation mesh. The experimental data from the first regime, characterized by a lower point density, are in good agreement with the calculations based on the knock-on model. Conversely, for the second regime the resistance of the irradiated material is strongly increased by irradiation, corresponding to a very large variation of the oxygen content that could not be reproduced by this model. This is likely because, for very close irradiation points and heavily irradiated samples, the assumptions that irradiations at different points are independent one from the other and that irradiation effects are simply additive are not valid. However, we cannot exclude that in this second regime other mechanisms besides the oxygen knock-on by secondary electrons can contribute to the observed variations.

Finally, by fitting the experimental data, we have estimated the value of the threshold displacement energy of interstitial oxygen atoms. The obtained value $T_d = 0.15^{+0.025}_{-0.01}$ eV is intermediate between previously reported values of activation energy for oxygen diffusion (T_d =0.93 eV [37]) and of threshold displacement energy for α-irradiation experiments (T_d =0.073 eV [38]), and is very close to the energy difference ΔE=0.2 eV between oxygen neighboring minima positions in the Bi-O layer, as determined by DFT calculations [42].

Acknowledgments

We gratefully acknowledge Elisabetta Durisi and Valeria Monti for fruitful discussions about MCNP6. This work has been carried out under partial financial support from project NANO-X jointly approved and funded by University of Torino and Compagnia di San Paolo. C.L. also acknowledges the Mega-grant of the Russian Federation Government (14.Y26.31.0001).

References

[1] G. F. Knoll, *Radiation detection and measurement* (John Wiley and Sons, 2010), fourth ed edn.

[2] F. Picollo, P. Olivero, F. Bellotti, Z. Pastuovic, N. Skukan, A. Lo Giudice, G. Amato, M. Jaksic, and E. Vittone, Diam. Relat. Mat. **19**, 466 (2010).

[3] B. Minetti, R. Gerbaldo, G. Ghigo, L. Gozzelino, F. Laviano, G. Lopardo, R. Cherubini, and E. Mezzetti, IEEE Trans. Appl. Supercond. **19**, 2882 (2009).

[4] V. Hardy, J. Provost, D. Groult, M. Hervieu, B. Raveau, S. Durcok, E. Pollert, J. C. Frison, J. P. Chaminade, and M. Pouchard, Physica C **191**, 85 (1992).

[5] J. Wiesner, C. Traeholt, J. G. Wen, H. W. Zandbergen, G. Wirth, and H. Fuess, Physica C **268**, 161 (1996).

[6] W. K. Kwok, U. Welp, A. Glatz, A. E. Koshelev, K. J. Kihlstrom, and G. W. Crabtree, Rep. Prog. Phys. **79**, 116501 (2016).

[7] L. Civale, A. D. Marwick, T. K. Worthington, M. A. Kirk, J. R. Thompson, L. Krusinelbaum, Y. Sun, J. R. Clem, and F. Holtzberg, Phys. Rev. Lett. **67**, 648 (1991).

[8] T. Terai, T. Kobayashi, K. Kishio, J. Shimoyama, S. Okayasu, and Y. Kazumata, Physica C **282**, 2135 (1997).

[9] K. Ogikubo, M. Nakano, T. Shitamichi, T. Terai, A. Yamawaki, S. Okayasu, and K. Hojou, Physica C **378**, 368 (2002).

[10] L. W. Lombardo, D. B. Mitzi, A. Kapitulnik, and A. Leone, Phys. Rev. B **46**, 5615 (1992).
[11] G. Blatter, M. V. Feigelman, V. B. Geshkenbein, A. I. Larkin, and V. M. Vinokur, Rev. Mod. Phys. **66**, 1125 (1994).
[12] H. Kumakura, H. Kitaguchi, K. Togano, H. Maeda, J. Shimoyama, S. Okayasu, and Y. Kazumata, J. Appl. Phys. **74**, 451 (1993).
[13] S. K. Tolpygo, J. Y. Lin, M. Gurvitch, S. Y. Hou, and J. M. Phillips, Phys. Rev. B **53**, 12462 (1996).
[14] F. Rullieralbenque, A. Legris, H. Berger, and L. Forro, Physica C **254**, 88 (1995).
[15] G. Aldica, F. Vasiliu, Geru, II, and B. M. Puscasu, J. Supercond. **13**, 623 (2000).
[16] A. De, N. R. Das, and S. N. Bhattacharyya, Jpn. J. Appl. Phys. Part 2 - Lett. **30**, L1873 (1991).
[17] T. Ishibashi, O. Yoda, and S. Goda, Physica C **228**, 379 (1994).
[18] W. Bras and H. Stanley, J. Non-Cryst. Solids **451**, 153 (2016).
[19] T. Isaji, T. Wakasugi, K. Fukumi, and K. Kadono, Chemical Physics Letters **522**, 72 (2012).
[20] V. Kiryukhin, D. Casa, J. P. Hill, B. Keimer, A. Vigliante, Y. Tomioka, and Y. Tokura, Nature **386**, 813 (1997).
[21] V. Duffort, V. Caignaert, V. Pralong, B. Raveau, M. R. Suchomel, and J. F. Mitchell, Solid State Commun. **182**, 22 (2014).
[22] A. Pagliero, L. Mino, E. Borfecchia, M. Truccato, A. Agostino, L. Pascale, E. Enrico, N. De Leo, C. Lamberti, and G. Martinez-Criado, Nano Lett. **14**, 1583 (2014).
[23] L. Mino, E. Borfecchia, A. Agostino, C. Lamberti, and M. Truccato, J. Electron Spectrosc., in press (2016).
[24] M. Truccato, A. Agostino, E. Borfecchia, L. Mino, E. Carat, A. Pagliero, N. Adhlakha, L. Pascale, L. Operti, E. Enrico, N. De Leo, M. Fretto, G. Martinez-Criado, and C. Lamberti, Nano Lett. **16**, 1669 (2016).
[25] L. Mino, V. Bonino, A. Agostino, C. Prestipino, E. Borfecchia, C. Lamberti, L. Operti, M. Fretto, N. De Leo, and M. Truccato, Scientific Reports **7**, 9, 9066 (2017).
[26] I. Pinera, C. M. Cruz, Y. Abreu, and A. Leyva, Phys. Status Solidi A-Appl. Mat. **204**, 2279 (2007).
[27] S. Cagliero, A. Agostino, E. Bonometti, and M. Truccato, Supercond. Sci. Technol. **20**, 667 (2007).
[28] S. Cagliero, A. Piovano, C. Lamberti, M. M. R. Khan, A. Agostino, G. Agostini, D. Gianolio, L. Mino, J. A. Sans, C. Manfredotti, and M. Truccato, J. Synchrotron Radiat. **16**, 813 (2009).
[29] T. Goorley, M. James, T. Booth, F. Brown, J. Bull, L. J. Cox, J. Durkee, J. Elson, M. Fensin, R. A. Forster, J. Hendricks, H. G. Hughes, R. Johns, B. Kiedrowski, R. Martz, S. Mashnik, G. McKinney, D. Pelowitz, R. Prael, J. Sweezy, L. Waters, T. Wilcox, and T. Zukaitis, Nuclear Technology **180**, 298 (2012).
[30] https://mcnp.lanl.gov/ (Accessed 26 July 2017).
[31] F. K. Seitz, J. S., in *Solid State Physics*, edited by F. T. Seitz, D. (Academic Press, New York, 1956), pp. 307.
[32] V. Petricek, Y. Gao, P. Lee, and P. Coppens, Phys. Rev. B **42**, 387 (1990).
[33] T. Watanabe, T. Fujii, and A. Matsuda, Phys. Rev. Lett. **79**, 2113 (1997).
[34] K. Inomata, T. Kawae, K. Nakajima, S. J. Kim, and T. Yamashita, Appl. Phys. Lett. **82**, 769 (2003).
[35] G. H. Kinchin and R. S. Pease, Rep. Prog. Phys. **18**, 1 (1955).
[36] M. Robinson, N. A. Marks, and G. R. Lumpkin, Phys. Rev. B **86**, 134105 (2012).
[37] M. Runde, J. L. Routbort, S. J. Rothman, K. C. Goretta, J. N. Mundy, X. Xu, and J. E. Baker, Phys. Rev. B **45**, 7375 (1992).
[38] S. K. Bandyopadhyay, P. Barat, P. Sen, A. K. Ghosh, A. N. Basu, and B. Ghosh, Phys. Rev. B **58**, 15135 (1998).

[39] S. K. Bandyopadhyay, A. K. Ghosh, P. Barat, P. Sen, A. N. Basu, and B. Ghosh, Physica Status Solidi a-Applied Research **162**, 701 (1997).
[40] S. K. Bandyopadhyay, P. T. Sen, P. Barat, P. Mukherjee, S. K. Das, and B. Ghosh, Pramana-Journal of Physics **47**, 309 (1996).
[41] C. Kendziora, L. Forro, D. Mandrus, J. Hartge, P. Stephens, L. Mihaly, R. Reeder, D. Moecher, M. Rivers, and S. Sutton, Phys. Rev. B **45**, 13025 (1992).
[42] Y. He, S. Graser, P. J. Hirschfeld, and H. P. Cheng, Phys. Rev. B **77**, 220507 (2008).